ELSEVIER

Journal of Power Sources 96 (2001) 293–302

JOURNAL OF POWER SOURCES

www.elsevier.com/locate/jpowsour

Effect of magnesium substitution on the cycling behavior of lithium nickel cobalt oxide

C. Pouillerie[a,b], F. Perton[b], Ph. Biensan[b], J.P. Pérès[b], M. Broussely[b], C. Delmas[a,*]

[a]*Institut de Chimie de la Matière Condensée de Bordeaux-CNRS and Ecole Nationale Supérieure de Chimie et Physique de Bordeaux, Château de Brivazac, Av. Dr A. Schweitzer, 33608 Pessac Cedex, France*

[b]*SAFT, Direction de la Recherche, 111 Bd. Alfred Daney, 33074 Bordeaux Cedex, France*

Received 4 September 2000; accepted 16 October 2000

Abstract

$LiNi_{0.91}Co_{0.09}O_2$ and $LiNi_{0.86}Co_{0.09}Mg_{0.05}O_2$ phases were comparatively cycled in 4/5 'A'-size lithium-ion cells (500 cycles, 60°C, C rate, 2 h floating at 4.1 V at each charge). The Mg–Co substituted positive electrodes exhibit a very small capacity fading versus the Co substituted one. Comparative Rietveld refinements of the XRD patterns before and after cycling show unambiguously that an irreversible migration of Mg^{2+} ions from the slabs to the interslab spaces occurs upon cycling. The variation of the cell parameters of the $Li_xNi_{0.86}Co_{0.09}Mg_{0.05}O_2$ deintercalated phases, obtained during the 1st and the 501st charges, were determined. The smaller changes observed after the Mg-migration suggest that the mechanical constraints typically observed during lithium intercalation–deintercalation are reduced by the simultaneous presence of magnesium ions in the lithium sites and of vacancies in the slabs, leading to a smaller capacity fading. © 2001 Elsevier Science B.V. All rights reserved.

Keywords: Lithium-ion batteries; Lithium batteries; Substituted lithium nickelate; Cycling; Rietveld refinement

1. Introduction

Due to its low cost and high energy density, $LiNiO_2$ has been considered as a promising positive electrode material for rechargeable lithium batteries [1–5]. However, this oxide is still not used in commercial cells, contrary to $LiCoO_2$, because of its tendency to give a higher capacity fading upon cycling [3,6,7] and of its lower thermal stability [7–10]. Since partial substitution for nickel is expected to improve the structural and electrochemical properties of lithium nickelate, we investigated the effect of magnesium and cobalt substitution on the cycling behavior of $LiNiO_2$. Two $LiNi_{0.91-y}Co_{0.09}Mg_yO_2$ phases ($y = 0$ and 0.05) were used as positive active materials in rechargeable lithium-ion batteries which were long-range cycled at 60°C (500 cycles at the C rate). The effect of the upper cutoff voltage on the capacity fading was also studied for $LiNi_{0.86}Co_{0.09}Mg_{0.05}O_2$. Detailed X-ray diffraction studies were then carried out to determine the structural evolution induced by the cycling process in order to explain the electrochemical behavior of the two $LiNi_{0.91-y}Co_{0.09}Mg_yO_2$ systems ($y = 0$ and 0.05).

2. Experimental

The $LiNi_{0.91}Co_{0.09}O_2$ phase was synthesized by direct reaction from oxides: a mixture of LiOH, NiO and Co_3O_4 powders (in the 1.05:0.91:0.09 molar ratio) was heated up to 690°C under dry oxygen for 15 h. The $LiNi_{0.86}Co_{0.09}Mg_{0.05}O_2$ phase was obtained by a hydroxide route, followed by a high temperature thermal treatment under dry oxygen at 750°C for 15 h.

The long cycle-life tests were performed in 4/5 'A'-size prototype lithium-ion cells (height = 42.4 mm; diameter = 16.6 mm) [3]. Graphite was used as negative electrode, the positive electrode consisted of the $LiNi_{0.91-y}Co_{0.09}Mg_yO_2$ phase ($y = 0$ or 0.05) as active material, polyvinylidiene fluoride (PVDF) (6% by weight) as binder and carbonblack (8%) as conductive agent. A solution of 1 M $LiPF_6$ in a mixture of propylene carbonate (PC), dimethyl carbonate (DMC) and ethylene carbonate (EC) (1:1:3 by volume) was used as electrolyte. A preliminary cell formation was

* Corresponding author. Tel.: +33-5-56-84-62-96; fax: +33-5-56-84-66-34.
E-mail address: delmas@icmcb.u-bordeaux.fr (C. Delmas).

PII: S0378-7753(00)00653-4

performed: five cycles were performed at room temperature at the C rate in the [2.7–4.0 V] potential range (with an intermediate floating of the cell during 2 h at 4.0 V), then the cells were stored during 8 days at 45°C. The C rate is defined as the exchange of 0.5 electrons in 1 h. This formation operation was performed four times. Five cycles were performed again at room temperature and 500 cycles were then carried out at 60°C, at the same rate and in the same potential range (which corresponds approximately to [2.8–4.1 V] versus lithium metal). At the end of each charge, an intermediate floating was also performed at 4.0 V during 2 h.

In order to determine the influence of the upper cutoff voltage on the cycling stability, coin cells using the magnesium substituted $LiNi_{0.86}Co_{0.09}Mg_{0.05}O_2$ phase as positive electrode material, a lithium negative electrode and 1 M $LiPF_6$ in PC/EC/DMC (1:1:3) as electrolyte, were cycled under the following experimental conditions: 60°C, C/20 rate in the [2.7–*y* V] potential range where the upper cutoff voltage *y* varied from 4.1 to 4.3 V.

$Li_xNi_{0.86}Co_{0.09}Mg_{0.05}O_2$ phases were obtained by electrochemical lithium deintercalation either from the pristine or from the 500-times-cycled materials. These experiments were carried out in lithium batteries exhibiting the following electrochemical chain: Li/1 M $LiPF_6$ in PC/EC/DMC (1:1:3)/positive electrode material without any additional conductive or organic binder (active mass ≈ 60 mg). The batteries were charged at the C/100 rate, with intermediate periods of relaxation, using a home made system monitored by a HP1000 computer, operating in a galvanostatic mode [11]. Lithium batteries with the $LiNi_{0.86}Co_{0.09}Mg_{0.05}O_2$ pristine phase as positive electrode material were also cycled in a potensiostatic mode between 3.4 and 4.3 V, with a rate of 10 mV/2 h (active mass of ≈40 mg) using a McPile system [12]. All the delithiated positive electrode materials were recovered in a dry box, washed in DMC to remove all traces of $LiPF_6$ salts and dried under vacuum.

The X-ray diffraction patterns (XRD) of all the materials were recorded using a Siemens D5000 powder diffractometer equipped with a diffracted beam monochromator (Cu Kα radiation). For the delithiated materials, the experiments were performed in a sample holder which avoids any contact of the oxidized positive electrodes with air. For routine X-ray diffraction analysis, the XRD patterns were collected in the 10–80° (2θ) range by steps of 0.02° (2θ) with a constant counting time of 10 s. For the structural characterization by the Rietveld method, the data were collected in the 5–120° (2θ) range with a counting time of 40 s at each 0.02° (2θ) step. The Rietveld refinements were carried out using the Fullprof program [13].

Whatever the real cationic distribution deduced from the refinement, the nominal compositions "$LiNi_{0.91}Co_{0.09}O_2$" and "$LiNi_{0.86}Co_{0.09}Mg_{0.05}O_2$" are used in this paper to designate the starting materials. For the deintercalated phases, the same types of formula are used with the lithium content deduced from the electrochemical study.

3. Results and discussion

3.1. Long range cycling experiments

The long-range cycling tests have been performed at 60°C, because high temperature cycling experiments are expected to accelerate the aging effects which are directly related to the electrochemical behavior of the electrode materials upon cycling.

Fig. 1 shows the evolution of the capacity recovered on discharge for the "$Li_xNi_{0.91-y}Co_{0.09}Mg_yO_2$" ($y = 0$ and 0.05) positive electrodes, during the long-rang cycling test performed at the C rate. A better capacity stability is obtained for $LiNi_{0.86}Co_{0.09}Mg_{0.05}O_2$, since only 10% of the capacity is lost between the 50th and the 500th cycles versus 40% for the "$LiNi_{0.91}Co_{0.09}O_2$" material. The capacity fading corresponds to an average decrease of 0.02 and 0.08% of the initial capacity per cycle for the Co–Mg and Co substituted systems, respectively. Note that the large capacity loss observed upon cycling for the "$LiNi_{0.91}Co_{0.09}O_2$" phase is similar to that previously reported for lithium nickelate [3,6]. These results show unambiguously that magnesium substitution improves significantly the cycling behavior of the cobalt substituted material.

3.2. Cycling experiments with various upper cutoff voltages

In order to emphasize the very good effect of magnesium substitution for nickel on the electrochemical stability of lithium nickel cobalt oxide, cycling tests were carried out, increasing the upper cutoff voltage, since it is well known that for "$LiNiO_2$", the capacity fading increases rapidly when the end of charge voltage increases.

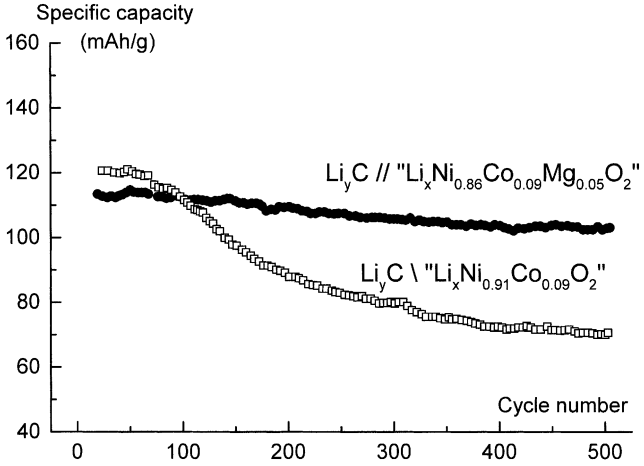

Fig. 1. Evolution of the specific capacity recovered on discharge for the "$Li_xNi_{0.91-y}Co_{0.09}Mg_yO_2$" ($y = 0$ and 0.05) positive electrodes during the long-range cycling test performed at 60°C, at the C rate. The first five cycles corresponding to the electrode formation and performed in different experimental conditions are not represented.

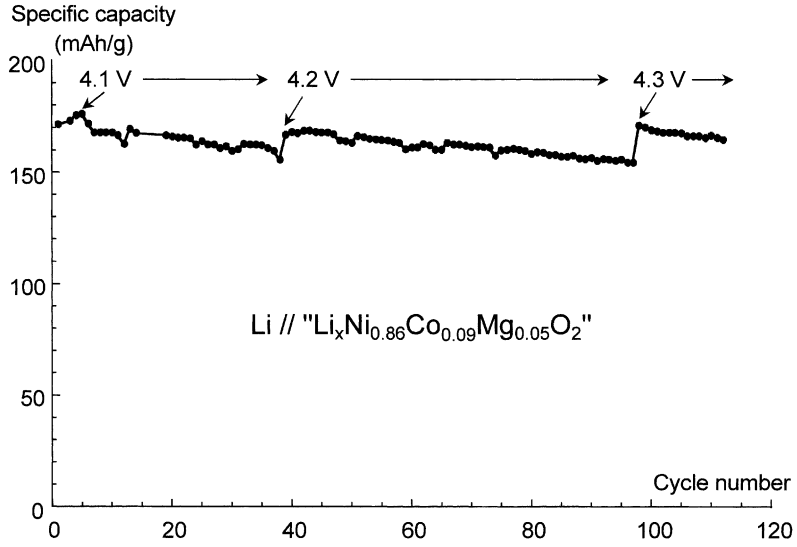

Fig. 2. Evolution of the capacity of the positive electrode "$Li_xNi_{0.86}Co_{0.09}Mg_{0.05}O_2$" upon cycling at 60°C; at the C/20 rate, in the [2.7–y V] potential range where the upper cutoff voltage y varied from 4.1 to 4.3 V.

Fig. 2 shows the evolution of the reversible capacity obtained for a Li//$Li_xNi_{0.86}Co_{0.09}Mg_{0.05}O_2$ coin cell upon cycling at the C/20 rate, at 60°C. The potential ranges (versus lithium metal) were [2.7–4.1 V] for the first 38 cycles, [2.7–4.2 V] between the 39th and 97th cycles and [2.7–4.3 V] for the last 15 cycles. A difference in specific capacity is observed between this experiment and the one reported above (Fig. 1), resulting from the difference in cycling rate and also from the difference in battery technology used in the two cases. A very small decrease of the reversible capacity is observed upon cycling whatever the upper cutoff voltage. Moreover, the slope of the curve is very similar for the three cycling domains, which shows that no increase of the capacity fading occurs when increasing the upper cutoff voltage. This result clearly demonstrates that magnesium substitution for nickel leads to an improvement of the cycling stability.

3.3. Structural modification upon cycling

3.3.1. X-ray diffraction analysis

A comparative structural study was performed on the Ni–Co and Ni–Co–Mg pristine phases and on the corresponding materials recovered after the long-range cycling test in order to determine if the difference in electrochemical behaviors between the two substituted systems results from different structural evolutions.

A preliminary X-ray diffraction analysis, performed on the positive electrode materials recovered after the 500th discharge, showed that the "$Li_xNi_{0.91}Co_{0.09}O_2$" phase crystallizes in the monoclinic system while the "$Li_xNi_{0.86}Co_{0.09}Mg_{0.05}O_2$" material exhibits the rhombohedral symmetry. The long-range-cycled electrodes were used to build new lithium cells, which were galvanostatically discharged at low rate (C/100) down to 2.7 V with intermediate relaxations, in order to try to come back to a composition close to the starting one. At the end of the discharge process, the composition of the two cycled materials was assumed to be close to $x \approx 0.90$. Since the scattering power of lithium is low, an accurate determination of the lithium composition was not required for the X-ray diffraction analysis.

Fig. 3 presents the XRD patterns of the cycled materials recovered at the end of the additional discharge, in comparison with those of the pristine phases. In both substituted systems, the crystallinity of the materials before and after the long-range cycling test is very good. However, we can notice that the diffraction lines appear to be slightly broader on the XRD patterns of the cycled materials. This observation is confirmed by the determination of the half-width of the (1 0 4) diffraction line (FWHM(1 0 4)) reported for all the materials on Fig. 3. Note that a smaller broadening of the diffraction lines was observed on the XRD pattern of the "$Li_{0.90}Ni_{1.03}O_2$" material recovered after 1200 cycles [3,14].

3.3.2. Rietveld refinement of the XRD patterns

These structural characterizations were realized on the pristine phases and on the long-range-cycled materials recovered after the additional discharge.

3.3.2.1. The pristine phases. For the "$LiNi_{0.91}CO_{0.09}O_2$" phase, the Rietveld refinement of its XRD pattern, including the site occupancy parameters and the isotropic thermal factors determination, showed that the material exhibits an ideal 2D structure, since no extra-cation was found in the interslab space. For the Co–Mg substituted material, assuming an ideal cationic distribution $[Li]_{3b}[Ni_{0.86}Co_{0.09}Mg_{0.05}]_{3a}O_2$, a negative value was obtained for the B(Li) isotropic parameter, giving evidence for an excess of electronic density in the lithium sites [15]. We showed previously

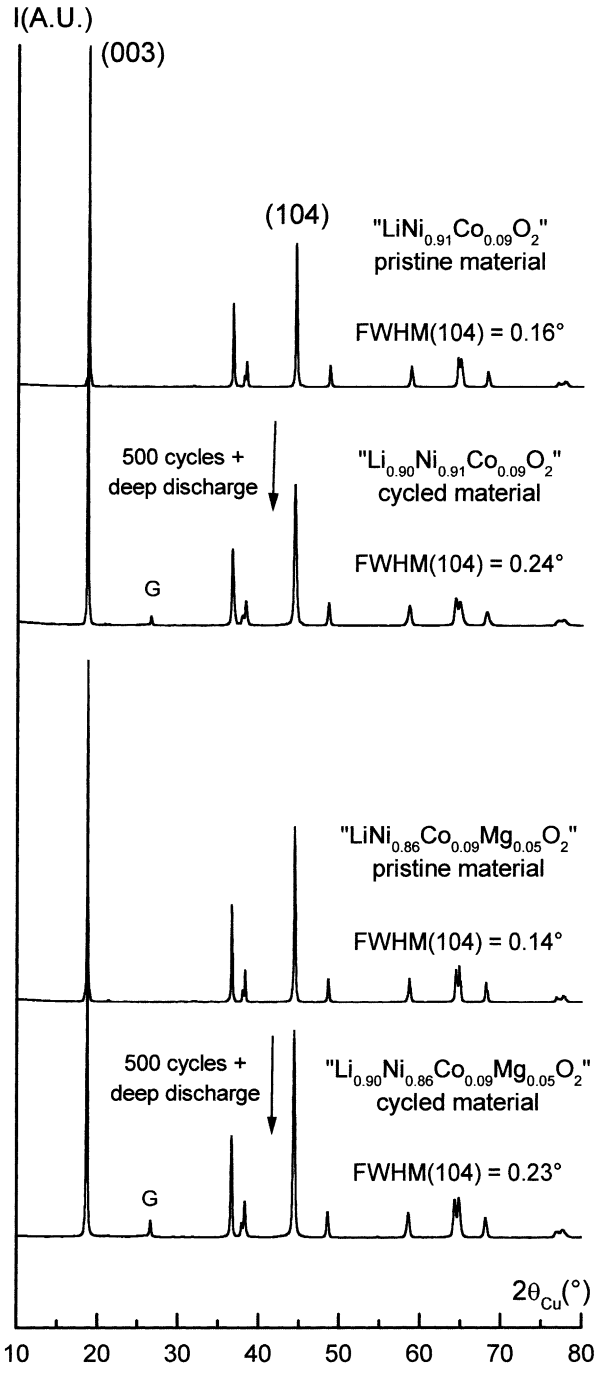

Fig. 3. XRD pattern of the "$Li_xNi_{0.91-y}Co_{0.09}Mg_yO_2$" ($y = 0$ and 0.05) pristine phases and of the corresponding 500-times-cycled materials recovered after an additional discharge. The half-width of the (1 0 4) diffraction line (FWHM(1 0 4)) is reported for all the XRD patterns.

that in the "$LiNi_{1-y}Mg_yO_2$" system ($0 \leq y \leq 0.20$) [16], if extra-cations are required in the interslab space for lithium deficiency compensation, magnesium ions occupy the lithium site preferentially to nickel ions, due to the difference in size between the various cations ($r_{Li^+} = 0.76$ Å, $r_{Mg^{2+}} = 0.72$ Å, $r_{Ni^{2+}} = 0.69$ Å, $r_{Ni^{3+}} = 0.56$ Å) [17]. Therefore, for "$LiNi_{0.86}Co_{0.09}Mg_{0.05}O_2$", the Rietveld refinement was carried out assuming the same structural model. About 2% of magnesium ions were determined to be located in the interslab space, leading to the real formula: $[Li_{0.98}Mg_{0.02}]_{3b}[Ni_{0.88}Co_{0.09}Mg_{0.03}]_{3a}O_2$. Note that this structure is very close to the ideal one. The results of the refinement are given for the two pristine phases in Table 1.

3.3.2.2. The 500-times-cycled materials. For the two long-range cycled materials, the Rietveld refinements of the XRD patterns were first performed assuming similar cationic distributions as those of the pristine phases: $[Li_{\text{``}0.90\text{''}}]_{3b}[Ni_{0.91}Co_{0.09}]_{3a}O_2$ and $[Li_{\text{``}0.90\text{''}}Mg_{0.02}]_{3b}[Ni_{0.88}Co_{0.09}Mg_{0.03}]_{3a}O_2$, respectively. In both cases, a negative value was obtained for the B(Li) isotropic atomic displacement parameter, showing that the amount of extra-cations in the interslab space had increased during the cycling process. Therefore, a cationic migration from the slab to the interslab space was considered. Such a cationic transfer was previously shown to take place in the "$Li_xNi_{0.90}Mg_{0.10}O_2$" system when the materials are oxidized at high potential upon cycling [18]. Since this cationic displacement requires a transfer through an intermediate tetrahedral site [1], the magnesium migration was expected to be easier than the nickel one, owing to the relative stabilities of magnesium and nickel ions in tetrahedral sites. Therefore, we assumed for the refinements a preferential magnesium transfer from the slab to the interslab space for "$Li_xNi_{0.86}Co_{0.09}Mg_{0.05}O_2$" and obviously a sole nickel migration for "$Li_xNi_{0.91}Co_{0.09}O_2$". In fact, in the first case, a small amount of Ni^{3+} ions was also considered to have migrated to the lithium sites upon cycling, since the presence of all the available magnesium ions in the interslab space only partially compensates for the excess of electronic density evidenced by the Rietveld refinement.

For both cycled materials, the main structural parameters are reported in Table 1, in comparison with those of the pristine phases. In all cases, the reliability factors are good, which underlines that the structural models considered describe fairly well the structure of the materials. For the "$Li_{0.90}Ni_{0.88}Co_{0.09}Mg_{0.05}O_2$" cycled material, the results of the refinement are also given in detail in Table 2. As shown in Fig. 4, the calculated pattern fits the experimental one quite well.

3.3.3. Evolution of the cationic distribution upon cycling

The results discussed above give evidence for the migration of all the magnesium ions and of an additional amount of 3% of nickel ions to the interslab space for the "$Li_xNi_{0.86}Co_{0.09}Mg_{0.05}O_2$" system, leading to the crystallographic formula $[Li_xMg_{0.05}Ni_{0.03}]_{3b}[Ni_{0.85}Co_{0.09}\square_{0.06}]_{3a}O_2$. A smaller change in cationic distribution occurs for the "$Li_xNi_{0.91}Co_{0.09}O_2$" system, since only 3% of nickel ions are observed in the lithium sites of the cycled cobalt-substituted material. In this case, the crystallographic formula is $[Li_xNi_{0.03}]_{3b}[Ni_{0.88}Co_{0.09}\square_{0.03}]_{3a}O_2$. This nickel migration seems relatively surprising since in the previous studies, starting from the $Li_{0.97}Ni_{1.03}O_2$ composition, no change in

Table 1
Crystallographic parameters, cationic distribution and reliability factors obtained from the Rietveld refinement of the XRD data of the "$Li_xNi_{0.91-y}Co_{0.09}Mg_yO_2$" ($y = 0$ and 0.05) pristine phases and of the corresponding long-range-cycled materials[a]

Nominal formula	a (Å)	c (Å)	$z_{ox.}$	Real formula	R_{wp} (%)	R_B (%)
"$LiNi_{0.91}Co_{0.09}O_2$" pristine material	2.8724 (2)	14.182 (1)	0.2592 (4)	$[Li_1][Ni_{0.91}Co_{0.09}]O_2$	11.0	1.99
"$Li_{0.90}Ni_{0.91}Co_{0.09}O_2$" recovered after 500 cycles	2.8700 (4)	14.230 (3)	0.2597 (6)	$[Li_{0.90}Ni_{0.03}][Ni_{0.88}Co_{0.09}\square_{0.03}]O_2$	10.1	3.00
"$LiNi_{0.86}Co_{0.09}Mg_{0.05}O_2$" pristine material	2.8739 (2)	14.204 (2)	0.2591 (6)	$[Li_{0.98}Mg_{0.02}][Ni_{0.88}Co_{0.09}Mg_{0.03}]O_2$	12.5	1.92
"$Li_{0.90}Ni_{0.86}Co_{0.09}Mg_{0.05}O_2$" recovered after 500 cycles	2.8746 (3)	14.242 (2)	0.2586 (4)	$[Li_{0.90}Mg_{0.05}Ni_{0.03}][Ni_{0.85}Co_{0.09}\square_{0.06}]O_2$	10.2	2.85

[a] The standard deviations were multiplied by the Scor parameter to correct from the local correlations [13].

Table 2
Results of the Rietveld refinement of the XRD pattern of the "$Li_{0.90}Ni_{0.86}Co_{0.09}Mg_{0.05}O_2$" long-range-cycled material[a]

Space group: R-3m
$a_{hex.} = 2.8746$ (3) Å; $c_{hex.} = 14.242$ (2) Å

Constraints
$n(Li) = 0.90$; $n(Co) = 0.09$; $n(Ni_1) + n(Ni_2) = 0.88$; $n(Mg_1) = 0.05$; $B(Li) = B(Mg_1) = B(Ni_1)$; $B(Ni_2) = B(Co)$

Conditions of the run
Temperature = 300 K; Angular range = $10^\circ \leq 2\theta \leq 120^\circ$; Step scan increment ($2\theta$) = 0.02°; Number of fitted parameters = 15

Profil parameters
Profil function: PV (Pseudo-Voigt) = $\eta L + (1-\eta)G$
$\eta = \eta_0 + X(2\theta)$; $\eta_0 = 0.37$ (4); $X = 0.003$ (1)

Halfwidth parameters
$U = 0.14$ (3); $V = 0.01$ (2); $W = 0.035$ (4)

Atoms	Site	Wyckoff positions			B_{iso} (Å^2)	Occupancy
Li	3b	0	0	1/2	1.0 (4)	0.90
Mg_1	3b	0	0	1/2	1.0 (4)	0.05
Ni_1	3b	0	0	1/2	1.0 (4)	0.025 (4)
Ni_2	3a	0	0	0	0.85 (6)	0.855 (4)
Co	3a	0	0	0	0.85 (6)	0.09
O	6c	0	0	0.2586 (4)	1.5 (1)	2.000

[a] The standard deviations were multiplied by the Scor parameter to correct from local correlations [13]. Conventional Rietveld R-factors for points with Bragg contribution: $R_{wp} = 10.2\%$; $R_B = 2.85\%$.

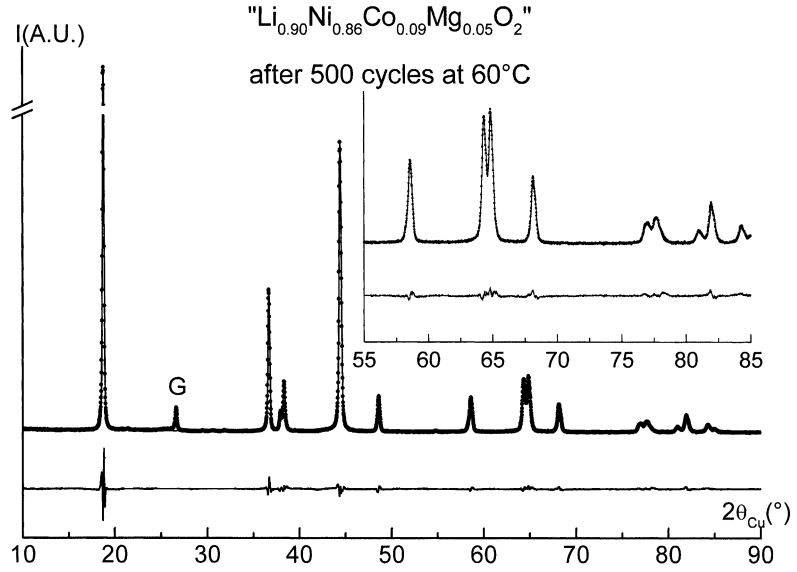

Fig. 4. Comparison of the experimental (●) and calculated (–) XRD patterns of the "$Li_{0.90}Ni_{0.86}Co_{0.09}Mg_{0.05}O_2$" 500-times-cycled material; the difference between experimental and calculated XRD pattern is also reported. The 90–120° (2θ) range is not represented to enlarge the figure.

the nickel distribution was detected after 1200 cycles [3,6,14]. In fact, the cycling conditions were quite different in the two studies. For the $Li_xNi_{1.03}O_2$ positive electrode material, 1200 cycles were performed at room temperature (charge C/2, discharge C) in the [2.7–4.15 V (versus lithium metal)] potential range, without any intermediate floating at high potential. On the contrary, for the substituted systems, 500 cycles were performed at 60°C (charge C, discharge C), in the [2.8–4.1 V (versus lithium metal)] potential range, with an intermediate floating at 4.1 V during 2 h at the end of each charge. In the latter experiments, the electrodes were maintained for a longer time at high potential in comparison to the first one. Therefore, nickel migration is expected to have been favored by the floating of the cells at high potential and by the higher temperature of the cycling test. Such a nickel migration was previously hypothesized to take place in the $Li_xNi_{1.02}O_2$ system during a long-time floating at high potential, but only when almost all the lithium ions are deintercalated [19].

3.3.4. Evolution of the structural parameters upon cycling

In order to confirm the cationic distributions deduced from the Rietveld refinement, we have compared in Table 3 the structural parameters of the materials before and after the cycling test with those of the $Li_{0.98}Ni_{1.02}O_2$ pristine phase and of the deintercalated $Li_{0.82}Ni_{1.02}O_2$ phase (obtained from a galvanostatic charge, at low rate). The slab thickness $S_{(NiO_2)}$ and the interslab thickness $I(LiO_2)$ correspond to the distances along the $c_{hex.}$ axis between the oxygen layers of the NiO_2 slab and of the LiO_2 interslab space, respectively. They are defined as $S_{(NiO_2)} = (2/3 - 2 \times z_{ox.}) \times c_{hex.}$ and $I_{(LiO_2)} = (C_{hex.}/3) - S_{(NiO_2)}$.

For the $Li_xNi_{1.02}O_2$ system, the deintercalation of the first 0.16 lithium ion from the structure of the pristine phase leads to classical modifications of the structural parameters. They consist of: on the one hand, a significant decrease of the $a_{hex.}$ intraslab distance, of the $d_{Ni–O}$ distance and of the $S_{(NiO_2)}$ slab thickness, resulting from the oxidation of a part of the Ni^{3+} ions to the smaller Ni^{4+} ions in the slabs, and on the other hand, a significant increase of the $c_{hex.}$ interslab distance, of the $d_{Li–O}$ distance and of the $I_{(LiO_2)}$ interslab thickness, related to the increase of the electrostatic repulsions between the slabs when lithium ions are deintercalated from the interslab space. For the "$Li_xNi_{0.91}Co_{0.09}O_2$" and "$Li_xNi_{0.86}Co_{0.09}Mg_{0.05}O_2$" systems, different structural evolutions are observed, even if the cycled materials exhibit relatively similar lithium compositions than that of the $Li_{0.82}Ni_{1.02}O_2$ one. This result emphasizes that different evolutions of the cationic distribution occurred during the electrochemical tests:

- For the "$Li_xNi_{0.91}Co_{0.09}O_2$" system, after 500 cycles, although the $c_{hex.}$ parameter increased at almost the same magnitude than in the "$Li_xNi_{1.02}O_2$" system, the increase of the interslab characteristic distances ($d_{Li–O}$ and $I_{(LiO_2)}$) and the decrease of the intraslab characteristic ones ($a_{hex.}$, $d_{Ni–O}$ and $S_{(NiO_2)}$) with lithium deintercalation are significantly smaller.
- For the "$Li_xNi_{0.86}Co_{0.09}Mg_{0.05}O_2$" system, the $c_{hex.}$ parameter also increased by the same magnitude but the values obtained for the $a_{hex.}$, $d_{Ni–O}$ and $d_{Li–O}$ parameters of the cycled material are almost the same as those of the pristine phase. Furthermore, surprisingly, the $I_{(LiO_2)}$ interslab thickness decreased while the $S_{(NiO_2)}$ slab thickness increased after the long-range cycling.

These evolutions of the structural parameters confirm unambiguously the cationic migration from the slab to the interslab space during the electrochemical process. Indeed, such a cationic transfer leads to the presence of Mg^{2+} and Ni^{3+} ions in the lithium sites, which implies a contraction of the interslab space, and therefore, smaller $I_{(LiO_2)}$ and $d_{Li–O}$ distances. Furthermore, it entails the formation of vacancies in the slabs which leads to an increase of the intraslab distances ($a_{hex.}$, $d_{Ni–O}$, $S_{(NiO_2)}$). Similar structural modifications related to cationic migrations were previously observed in the $Li_xNi_{0.92}Mg_{0.10}O_2$ system upon cycling [18] and also in the $Li_xNi_{1.02}O_2$ one [19] but at the very end of the lithium deintercalation process. The cationic transfer is related to the strong local constraints induced in the slabs by the difference in size between the various cations present in the charged state ($r_{Mg^{2+}} = 0.72$ Å, $r_{Ni^{3+}} = 0.56$ Å, $r_{Ni^{4+}} = 0.48$ Å, $r_{Co^{3+}} = 0.525$ Å). The large Mg^{2+} ions and to a smaller extent the Ni^{3+} ions in the 3a sites are destabilized in the very oxidized materials, since the interatomic intraslab distances are mainly imposed by the size of the prevailing Ni^{4+} ions.

Table 3
Comparison of the structural parameters of various pristine and deintercalated materials ($a_{hex.}$ and $c_{hex.}$ cell parameters, average Ni–O and Li–O distances, thickness of the $S_{(NiO_2)}$ slab layer and $I_{(LiO_2)}$ interslab space)

Compounds	$a_{hex.}$ (Å)	$c_{hex.}$ (Å)	$d_{Ni–O}$ (Å)	$d_{Li–O}$ (Å)	$S_{(NiO_2)}$ (Å)	$I_{(LiO_2)}$ (Å)
"$Li_{0.98}Ni_{1.02}O_2$" uncycled	2.8768 (1)	14.1892 (5)	1.971 (2)	2.111 (2)	2.132	2.598
"$Li_{0.82}Ni_{1.02}O_2$" from a single charge	2.8670 (1)	14.2374 (6)	1.954 (2)	2.127 (2)	2.074	2.672
"$LiNi_{0.91}Co_{0.09}O_2$" uncycled	2.8724 (2)	14.182 (1)	1.964 (3)	2.115 (4)	2.103	2.625
"$Li_{0.90}Ni_{0.91}Co_{0.09}O_2$" after 500 cycles at 60°C	2.8700 (4)	14.230 (3)	1.960 (4)	2.121 (5)	2.096	2.648
"$LiNi_{0.86}Co_{0.09}Mg_{0.05}O_2$" uncycled	2.8739 (2)	14.204 (2)	1.966 (4)	2.116 (5)	2.109	2.626
"$Li_{0.90}Ni_{0.86}Co_{0.09}Mg_{0.05}O_2$" after 500 cycles at 60°C	2.8746 (3)	14.242 (2)	1.972 (3)	2.114 (3)	2.129	2.619
"$Li_{0.92}Ni_{0.86}Co_{0.09}Mg_{0.05}O_2$" after one cycle with 360 h floating at 4.3 V	2.8746 (3)	14.217 (2)	1.968 (4)	2.116 (4)	2.111	2.628

3.4. Structural modification observed after a floating at high potential

A lithium battery with the "$LiNi_{0.86}Co_{0.09}Mg_{0.05}O_2$" starting phase as positive electrode material was potensiostatically charged up to 4.3 V (10 mV/2 h). The cell voltage was maintained at this potential during 360 h. The cell was then discharged down to 3.4 V with a final floating at this potential in order to try to come back to a composition close to the starting one. The electrochemical study showed that the composition of the recovered material is close to "$Li_{0.92}Ni_{0.86}Co_{0.09}Mg_{0.05}O_2$"; nevertheless, a small uncertainty on the lithium content exists due to the slight electrolyte oxidation at high potential, which cannot be completely avoided.

A detailed structural characterization of the positive electrode material recovered at the end of this electrochemical process was then performed by the Rietveld refinement of its XRD pattern. The results are reported in Table 4. Fig. 5 shows the good agreement obtained between the experimental and the calculated patterns. Assuming that magnesium migration from the slab to the interslab space is easier than the nickel one, the Rietveld analysis gives evidence for the transfer of all the magnesium ions to the lithium sites during the electrochemical experiment, leading to the cationic distribution $[Li_{0.92}Mg_{0.05}]_{3b}[Ni_{0.88}Co_{0.09}\square_{0.03}]_{3a}O_2$ (Table 4). From a general point of view, the structural parameters of this phase are intermediate between those of the pristine phase and of the 500-cycled material (Table 3), in agreement with the smaller cationic migration in this material in comparison to the 500-times-cycled one.

3.5. Origin of the suppression of the capacity fading with the magnesium substitution

As shown above, partial magnesium substitution for nickel stabilizes considerably the cycling performances of the "$LiNi_{0.86}Co_{0.09}Mg_{0.05}O_2$" phase, since no improvement of the cycling life was shown for the "$Li_xNi_{0.91}Co_{0.09}O_2$" system versus non substituted lithium nickelate. The structural study clearly gives evidence for the magnesium migration from the slab to the interslab space during the long-cycle life test in the Co–Mg substituted system, which entails a significant modification of the structural parameters. Therefore, one can assume that this cationic transfer is responsible for the strong reduction of the capacity fading upon cycling.

Indeed, as Mg^{2+} ions do not participate in the electrochemical process and as their size is very close to the Li^+ one, the Mg^{2+} ions localized in the lithium sites do not induce any local collapse of the interslab spaces, which would hinder the lithium diffusion during the cycling process, as observed for the $Li_{1-z}Ni_{1+z}O_2$ systems [20,21]. Furthermore, in the $Li_xNi_{1-y}Mg_yO_2$ system, we discussed previously that the magnesium migration must limit the changes of the cell parameters during the charge–discharge process, in relation to the strong screening and steric effects induced by the presence of magnesium ions in the interslab spaces and of vacancies in the slabs [18]. These cell parameters changes were recently associated to electrode damages upon cycling for the Li_xNiO_2 and Li_xCoO_2 systems, which are certainly responsible for a loss of contact between crystallites within the electrode, leading to an increase of the electrode impedance [22–25].

Table 4
Results of the Rietveld refinement of the XRD pattern of the "$Li_{0.92}Ni_{0.86}Co_{0.09}Mg_{0.05}O_2$" phase recovered after a potensiostatic cycle of the Li// $Li_xNi_{0.86}Co_{0.09}Mg_{0.05}O_2$ cell in the 3.4–4.3 V voltage range, with an intermediate floating at 4.3 V during 360 h[a]

Space group: *R*-3*m*
$a_{hex.} = 2.8746\ (1)$ Å; $c_{hex.} = 14.217\ (1)$ Å

Constraints
$n(Li) = 0.92$; $n(Co) = 0.09$; $n(Ni_1) + n(Ni_2) = 0.88$; $n(Mg_1) = 0.05$; $B(Li) = B(Mg_1) = B(Ni_1)$; $B(Ni_2) = B(Co)$

Conditions of the run
Temperature = 300 K; Angular range = $10^\circ \le 2\theta \le 120^\circ$; Step scan increment ($2\theta$) = 0.02°; Number of fitted parameters = 15

Profil parameters
Profil function: PV (Pseudo-Voigt) = $\eta L + (1-\eta)G$
$\eta = \eta_0 + X(2\theta)$; $\eta_0 = 0.57\ (5)$; $X = 0.001\ (1)$

Halfwidth parameters
$U = 0.12\ (2)$; $V = -0.04\ (2)$; $W = 0.031\ (3)$

Atoms	Site	Wyckoff positions			B_{iso} (Å^2)	Occupancy
Li	3b	0	0	1/2	1.1 (6)	0.92
Mg_1	3b	0	0	1/2	1.1 (6)	0.05
Ni_1	3b	0	0	1/2	1.1 (6)	0.004 (4)
Ni_2	3a	0	0	0	0.93 (8)	0.876 (4)
Co	3a	0	0	0	0.93 (8)	0.09
O	6c	0	0	0.2591 (6)	1.5 (2)	2.000

[a] The standard deviations were multiplied by the Scor parameter to correct from local correlations [13]. Conventional Rietveld *R*-factors for points with Bragg contribution $R_{wp} = 9.63\%$; $R_B = 3.78\%$.

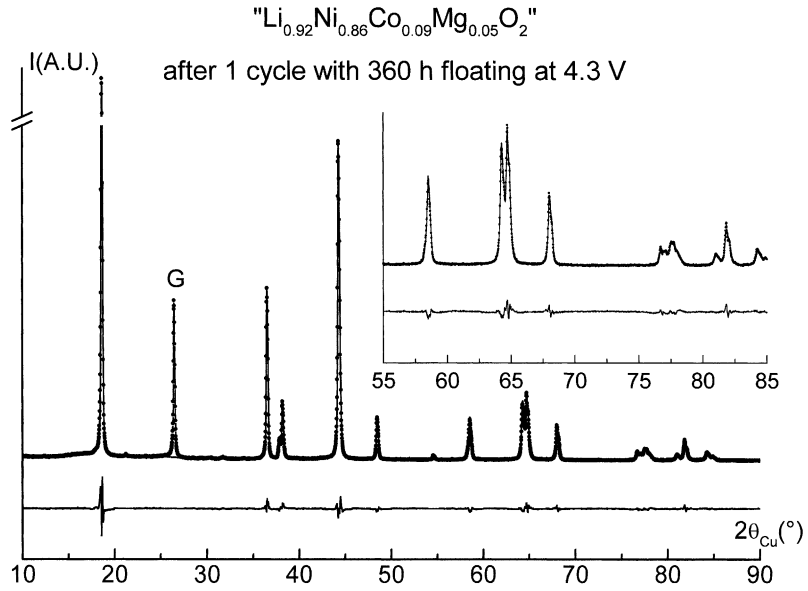

Fig. 5. Comparison of the experimental (●) and calculated (–) XRD patterns for the "$Li_{0.92}Ni_{0.86}Co_{0.09}Mg_{0.05}O_2$" phase recovered after one potensiostatic cycle with an intermediate floating at 4.3 V during 360 h; the difference between experimental and calculated XRD pattern is also reported. The 90–120° (2θ) range is not represented to enlarge the figure.

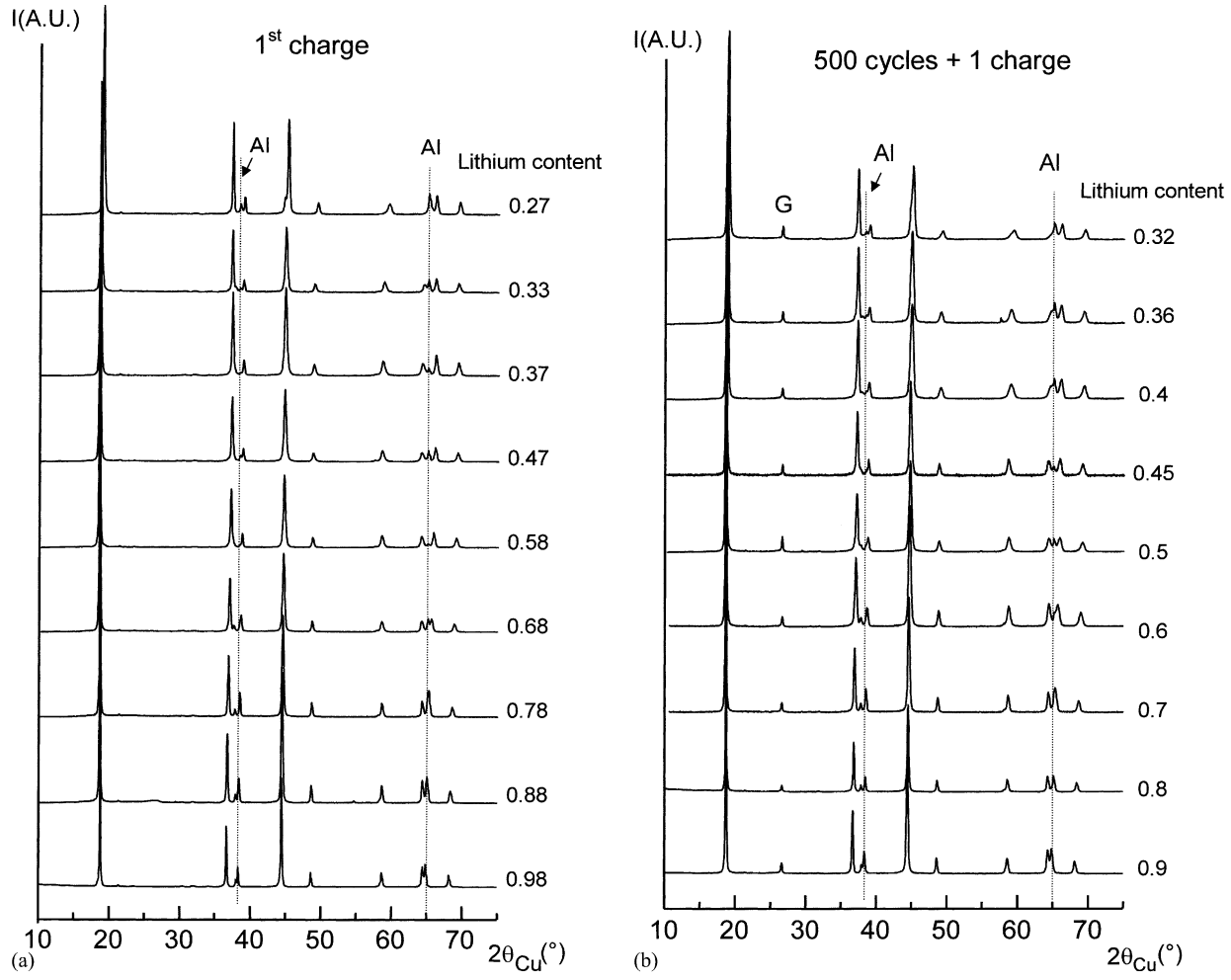

Fig. 6. XRD patterns of the "$Li_xNi_{0.86}Co_{0.09}Mg_{0.05}O_2$" deintercalated phases obtained by electrochemical deintercalation from the "$LiNi_{0.86}Co_{0.09}Mg_{0.05}O_2$" pristine phase (a) and from the "$Li_{0.90}Ni_{0.86}Co_{0.09}Mg_{0.05}O_2$" long-range-cycled material (b). No phase transition is observed during the charging process for both magnesium-substituted materials.

A detailed structural characterization was performed on the "$Li_xNi_{0.86}Co_{0.09}Mg_{0.05}O_2$" phases, obtained by electrochemical deintercalation from the pristine phase and from the 500-times-cycled material. The aim of this study was to determine the evolution of the cell parameters during the first charge (when a very small amount of magnesium ions is present in the interslab space) and during the 501st charge (when all the magnesium ions are located in the lithium sites). As mentioned in the experimental part, the deintercalated phases were obtained from lithium laboratory cells, galvanostatically charged at low rate (C/100) with intermediate periods of relaxation to avoid strong polarization of the batteries, since the positive electrodes were built without any additional binder or conductive agent.

Fig. 6a and b presents the XRD patterns of the "$Li_xNi_{0.86}Co_{0.09}Mg_{0.05}O_2$" deintercalated phases ($0.25 < x < 1$) recovered during the 1st and 501st charges, respectively. In both cases, all the materials crystallize in the rhombohedral system in agreement with the existence of a solid solution in the overall composition range [16]. As shown in Fig. 7, the variation of the hexagonal cell parameters of the deintercalated phases appears to be significantly limited during the 501st charge compared to that observed during the 1st charge. Between $x = 0.45$ and 0.90, which correspond approximately to the limit lithium compositions achieved during the long-range cycling experiment (126 mA h/g), the relative changes in the $a_{hex.}$ and $c_{hex.}$ parameters are both equal to 1.4% at the 1st charge, while they are equal to 1.3 and 0.7%, respectively at the 501st charge. One must notice that the cell parameters variations at the 1st charge are very similar to those reported by Saadoune and Delmas for the $Li_xNi_{0.8}Co_{0.2}O_2$ system [26]. The presence of a larger amount of extra-cations in the interslab space after the long-range cycling process tends to increase the $c_{hex.}$ parameter in the discharged state (steric effects) and to decrease it in the charged state (oxygen–oxygen screening effect). Simultaneously, the presence of cationic vacancies in the MO_2 slab tends to increase the M–M distance and to prevent also the lattice contraction induced by the cationic oxidation. These effects lead to a reduction of the changes in cell parameters upon cycling.

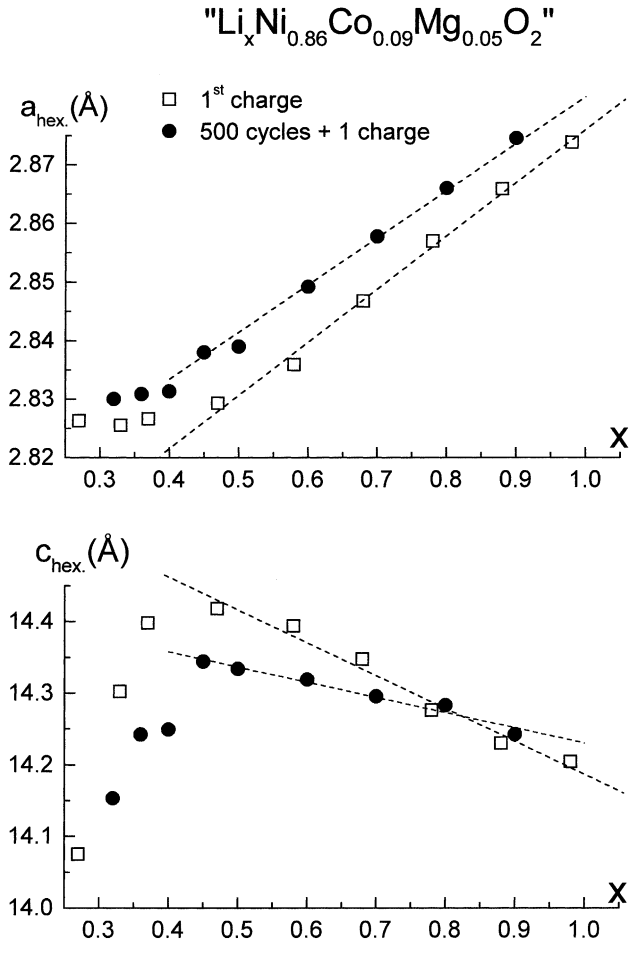

Fig. 7. Variation of the $a_{hex.}$ and $c_{hex.}$ cell parameters versus lithium amount x for "$Li_xNi_{0.86}Co_{0.09}Mg_{0.05}O_2$" during the 1st charge (□) (when a minority of magnesium ions are present in the interslab spaces) and during the 501st charge (●) (when all the magnesium ions are located in the interslab spaces).

4. Conclusion

The presence of a very small amount of magnesium in cobalt-substituted lithium nickelate allows to decrease to a large extent the capacity fading upon cycling. Due to the difference in ionic radius between Mg^{2+} and Ni^{4+} ions, the Mg^{2+} ions are destabilized within the slabs and then migrate to the interslab space during the charge process. As a result of this change in cationic distribution, the variation of the cell parameters upon cycling is significantly reduced, which limits the decohesion between crystallites, which are responsible for local electrode damages and for capacity fading.

Acknowledgements

The authors wish to thank V. Prevost and B. Delatouche for technical assistance, M. Ménétrier and L. Croguennec for fruitful discussions and Région Aquitaine and CEE (Contract CT960064) for financial support.

References

[1] M.G.S.R. Thomas, W.I.F. David, J.B. Goodenough, P. Groves, Mater. Res. Bull. 20 (1985) 1137.
[2] M. Broussely, F. Perton, J. Labat, R.J. Staniewicz, A. Romero, J. Power Sources 43/44 (1993) 209.
[3] M. Broussely, F. Perton, P. Biensan, J.M. Bodet, J. Labat, A. Lecerf, C. Delmas, A. Rougier, J.P. Pérès, J. Power Sources 54 (1995) 109.
[4] J.R. Dahn, U. Von Sacken, M.W. Juzkow, H. Al-Janaby, J. Electrochem. Soc. 138 (1991) 2207.
[5] T. Ohzuku, A. Ueda, Solid State Ionics 69 (1994) 201.
[6] C. Delmas, J.P. Pérès, C. Louchet, F. Weill, M. Broussely, F. Perton, P. Biensan, A. de Guibert, P. Willmann, in: Extended Abstracts of the

Proceedings of the 9th International Meeting on Lithium Batteries, Poster II, 1998, p. 38.
[7] M. Broussely, P. Biensan, B. Simon, Electrochim. Acta 45 (1999) 3.
[8] J.R. Dahn, E.W. Fuller, M. Obrovac, U. Von Sacken, Solid State Ionics 69 (1994) 265.
[9] T. Ohzuku, A. Ueda, M. Kouguchi, J. Electrochem. Soc. 142 (1995) 4033.
[10] H. Arai, S. Okada, Y. Sakurai, J. Yamaki, Solid State Ionics 109 (1998) 295.
[11] A. Mendiboure, C. Delmas, Comput. Chem. 11 (1987) 153.
[12] C. Mouget, Y. Chabre, McPile, licensed from CNRS and UW Grenoble to BIO-LOGIC Co., 1 av. de l'Europe, F-38640 Claix.
[13] J. Rodriguez-Carvajal, in: Proceedings of the Satellite Meeting on Powder Diffraction of the XV Congress of the IUCr, 1990, p. 127.
[14] C. Delmas, F. Perton, P. Biensan, M. Broussely, J. Power Sources, submitted for publication.
[15] A. Rougier, P. Gravereau, C. Delmas, J. Electrochem. Soc. 143 (1996) 1168.
[16] C. Pouillerie, L. Croguennec, P. Biensan, P. Willmann, C. Delmas, J. Electrochem. Soc. 147 (2000) 2061.
[17] R.D. Shannon, C.T. Prewitt, Acta Cryst. B25 (1969) 925.
[18] C. Pouillerie, L. Croguennec, C. Delmas, Solid State Ionics 132 (2000) 15.
[19] L. Croguennec, C. Pouillerie, C. Delmas, J. Electrochem. Soc. 147 (2000) 1314.
[20] J.P. Pérès, C. Delmas, A. Rougier, M. Broussely, F. Perton, P. Biensan, P. Willmann, J. Phys. Chem. Solids 57 (1996) 1057.
[21] C. Delmas, J.P. Pérès, A. Rougier, A. Demourgues, F. Weill, A. Chadwick, M. Broussely, F. Perton, P. Biensan, P. Willmann, J. Power Sources 68 (1997) 120.
[22] S. Waki, K. Dokko, T. Matsue, I. Uchida, Denki Kagaku 65 (1997) 954.
[23] H.F. Wang, Y.I. Jang, B.Y. Huang, D.R. Sadoway, Y.T. Chiang, J. Electrochem. Soc. 146 (1999) 473.
[24] T. Maegawa, A. Nozaki, S. Miyashita, F. Uchikawa, Electrochemistry 67 (1999) 1054.
[25] C. Louchet Pouillerie, Thesis, University of Bordeaux I, 2000.
[26] I. Saadoune, C. Delmas, J. Solid State Chem. 136 (1998) 8.